

Article

Effect of Thermal Radiation and Variable Viscosity on Bioconvective and Thermal Stability of Non-Newtonian Nanofluids under Bidirectional Porous Oscillating Regime

Lioua Kolsi ¹, Kamel Al-Khaled ², Sami Ullah Khan ^{3,*} and Nidhal Ben Khedher ¹

¹ Department of Mechanical Engineering, College of Engineering, University of Ha'il, Ha'il City 81451, Saudi Arabia

² Department of Mathematics & Statistics, Jordan University of Science and Technology, P.O. Box 3030, Irbid 22110, Jordan

³ Department of Mathematics, Namal University, Mianwali 42250, Pakistan

* Correspondence: samiullah@namal.edu.pk

Abstract: The bioconvective flow of a Jeffrey fluid conveying tiny particles under the effect of an oscillating stretched bidirectional surface is considered in this paper. The effects of thermal radiation and a porous medium are also investigated. The Cattaneo–Christov diffusion theories are used to analyze the heat and mass transfer phenomena. The activation energy effects are included in the concentration equation. The solved dimensionless equations system is established, based on non-dimensional variables. The analytical findings are evaluated using the homotopic analysis technique. The convergence of solutions is ensured. The results are validated by already available published findings and a good concordance is encountered. The fundamental physical aspect of flow parameters is graphically evaluated. The main results reveal that the velocity is reduced by increasing the permeability of the porous medium. An increase in the temperature occurs when the viscosity of the fluid is varied. The obtained results can be useful in thermal systems, energy production, heat transfer devices, solar systems, biofuels, fertilizers, etc.

Keywords: Jeffrey fluid; tiny particles; gyrotactic microorganisms; Cattaneo–Christov double diffusion; bidirectional oscillating surface

MSC: 76E06



Citation: Kolsi, L.; Al-Khaled, K.; Khan, S.U.; Khedher, N.B. Effect of Thermal Radiation and Variable Viscosity on Bioconvective and Thermal Stability of Non-Newtonian Nanofluids under Bidirectional Porous Oscillating Regime. *Mathematics* **2023**, *11*, 1600. <https://doi.org/10.3390/math11071600>

Academic Editor:
Umberto Morbiducci

Received: 7 March 2023
Revised: 22 March 2023
Accepted: 24 March 2023
Published: 26 March 2023



Copyright: © 2023 by the authors. Licensee MDPI, Basel, Switzerland. This article is an open access article distributed under the terms and conditions of the Creative Commons Attribution (CC BY) license (<https://creativecommons.org/licenses/by/4.0/>).

1. Introduction

A nanofluid represents a suspension of nanoparticles in a base fluid. These new kinds of engineered fluids are characterized by their enhanced thermophysical properties. Several studies have been performed on the enhancement of thermal processes using nanofluids. Nanofluids can be used to improve the heat transfer in various engineering systems, such as energy production, extrusion processes, solar systems, etc. The first research on nanofluids was performed by Choi [1]. Boungrino [2] reported the thermophoretic and Brownian motion of a nanofluid model. Mahmud et al. [3] investigated the effect of the Lorentz force on the cross-diffusion flow of a couple stress nanofluid over a porous Riga plate. It was mentioned that the Lorentz force effectively controls the fluid flow and enhances the heat transfer. Madkhali et al. [4] studied the mixed convective heat transfer of the Maxwell hybrid nanofluid using the generalized Fourier and Fick laws. The main findings reveal that the rate of the heat transfer is more important using a hybrid nano-Maxwell fluid compared to the pure Maxwell fluid. Hameed et al. [5] studied the combined effects' heat generation/absorption, magnetic field, and viscous dissipation on the couple stress Casson hybrid nanofluid flow across a nonlinear stretching surface. A reduction in the fluid velocity is noticed when the coupled stress fluid parameter is increased. Chandrasekaran et al. [6] performed an experimental

study on the heavy-duty engine radiator with the use of a cerium oxide nanofluid. It was observed that the heat transfer capability of automobile radiators was improved with the use of a cerium oxide-based nanofluid. This improves the radiator performances and engine efficiency by enhancing the heat exchange. Cui et al. [7] investigated the effects of non-identical modeling for a forced convection study of the nanofluid flow across stretching sheets under the effects of a chemical reaction and heat generation. It was found that the heat generation increases the heat transfer more compared to the chemical reaction. Mishra et al. [8] considered the buoyancy-driven flow of a non-Newtonian nanofluid around a moving sphere. It was observed that a separation in velocity is associated to the pulsating flow. Mahmud et al. [9] studied the nanofluid flow with magnetic shear thinning and Hall current effects. The solution of the governing equation was predicted based on the zero-mass flux constraints. A fluctuation in the oblique stagnation point flow was noticed when the ion-slip and Hall effects are considered. Balaji et al. [10] examined the enhanced heat transfer properties of water-based hybrid nanofluids containing multiwall carbon nanotubes and graphene nanoplatelets. It was found that the heat transfer rate was more important for graphene nanoplatelets. Manohar et al. [11] considered the dynamics of the hybrid nanofluid passing through a porous, semi-sphere-shaped fin under the effect of internal heat production. Chen et al. [12] investigated the natural convection of nanofluids under the influence of a variable-direction electrical field. Zheng et al. analyzed the heat transfer and fluid flow corrugated double-tube heat exchanger working with nanofluids. The results show that the use of nanoparticles has significant potential to improve the thermal performance of double-tube heat exchangers. Jaafar et al. [13] discussed the opposing flow phenomenon with a porous space subject to the hybrid nanofluid. Mustafa et al. [14] highlighted the applications of nanofluids in the cooling of LEDs with the help of heat exchangers. Zainal et al. [15] classified the hybrid nanofluid thermal outcomes via numerical simulations. The parallel surface flow with an injection impact due to the interaction of nanoparticles has been focused on by Abdollahi et al. [16].

The phenomenon known as bioconvection is the macroscopic convective motions caused by density variations in a suspension of swimming microorganisms. These motile bacteria can be categorized as oxytactic, gyrotactic, chemotactic, or gravitactic, depending on the cause to which the movement of the bacterium is a response. The process intensification involving correct mixing caused by the thermo-fluidic transport process and mass transfer rate occurs in several industries and in medical science. Shahzad et al. [17] studied the bioconvective micropolar nanofluid flow between double discs with the Cattaneo–Christov heat flux, which is affected by Brownian motion and thermophoretic diffusion. Kairi et al. [18] studied the thermo-solutal Marangoni bioconvective flow of gyrotactic bacteria suspended in a Williamson nanofluid. It was concluded that a higher heat transfer rate occurs when the Marangoni parameter is increased. Hussain et al. [19] investigated the bioconvection of oxytactic microorganisms suspended with a nano-encapsulated phase change material in a porous enclosure. Din et al. [20] studied the bioconvective heat transfer of nanofluid over a moving wedge. Mariam et al. [21] numerically investigated the heat transfer and flow fluid of a nanofluid suspended with microorganisms. Cui et al. [22] studied the bioconvection flow of Oldroyd-B fluid over a flat surface under the effects of a chemical reaction and heat generations. Habib et al. [23] studied the bioconvection and mass transpiration of micropolar nanofluids over an extended surface with a focus on the thermal radiation effect. It was mentioned that a higher Peclet number leads to the reduction in the microorganism's concentration. Waqas et al. [24] investigated the bioconvective flow of a Casson nanofluid over a spinning disc while considering the slip effects. It was concluded that the presence of slip features enhances the heat transfer considerably.

The non-Newtonian fluids are inspired materials with a novel and complex rheology. The dynamic of such non-Newtonian materials is interesting and unique. Different applications of such materials are predicted in biological systems, chemical industries, mechanical systems, food industries, and manufacturing systems. Moreover, the non-Newtonian fluids are of marvelous importance in cosmetics, medicines, wire drawing, plastic processes, blood, etc. Due to the specified rheology, different constitutive equations are presented to

justify the non-Newtonian models. The Jeffrey fluid model is one famous model which attracted the attention of researchers in recent years. The rheology of the Jeffrey model is associated to three factors, namely the viscosity, relaxation to retardation time ratio, and retardation time factor. The Jeffrey fluid model captured the memory features and elastic effects associated to the dilute polymer solutions [25]. The constitutive relation for this model is presented via extra stress tensor \mathbf{S} as

$$\mathbf{S} = \frac{\mu}{(1 + \Omega)} \left[\mathbf{A} + \alpha_* \left(\frac{\partial \mathbf{A}}{\partial t} + (\mathbf{V} \cdot \nabla) \mathbf{A} \right) \right], \quad (1)$$

With material dynamic viscosity (μ), retardation time factor (α_*), and relaxation to retardation times ratio (Ω). The scientists have performed different studies by using the Jeffrey fluid model. Muzara and Shateyi [26] tested the viscous dissipation impact for the Jeffrey fluid with the heat source impact. Raje et al. [27] reported the optimized estimation for a pipe flow with Jeffrey material. Khan et al. [28] worked out analytical computations for the Jeffrey fluid flow by using the latest Prabhakar scheme. The thermo-diffusion phenomenon for the Jeffrey material confining the unsteady flow was reported by Mushtaq et al. [29]. Ahmad et al. [30] discussed the three-dimensional flow of the Jeffrey nanofluid with an oscillating regime.

Based on the above presented literature review, it can be concluded that the bioconvective flow of nanofluids has been the subject of several studies. However, the investigation of the bioconvection of the Jeffrey fluid conveying tiny particles in view of variable thermal conductivity has not been reported yet. In the current study, the flow is induced by a bidirectional oscillatory stretching surface instead of a linearly stretched surface. To avoid the turbulent phenomenon, the magnitude of the oscillations was kept small. In addition, the effects of the porous medium and thermal radiation are depicted. The motivations for considering the Jeffrey nanofluid are due to its important rheological features as well as its potential industrial and engineering applications. The formulated problem is solved with the homotopy analysis method. The physical dynamics of this problem are presented via different tables and graphs.

2. Problem Formulation

An unsteady bidirectional flow caused by periodically moving porous surface of Jeffrey fluid conveying tiny particles is considered. The flow is induced by a periodically moving surface having bidirectional velocities $u = U_{\tilde{x}} = a\tilde{x} \sin \omega t$ and $v = V_{\tilde{y}} = b\tilde{y} \sin \omega t$ along with \tilde{x} - and \tilde{y} -directions, respectively (Figure 1). Here, a, b are the stretching rates while the ω indicates the angular frequency. The unsteady flow is induced by periodically moving surface at $\tilde{z} \geq 0$. The thermal conductivity of the fluid is assumed to be variable. The analysis of thermal and mass transfer features is based on the modified diffusion theories. The thermal radiation effect is also considered in the heat equation. The concentration equation is modified by using the activation energy features by using the Arrhenius equation. Additionally, the moving surface is maintained at a uniform temperature $\bar{T}_{\tilde{w}}$, microorganisms' density $\bar{N}_{\tilde{w}}$, and nanoparticles concentration $\bar{C}_{\tilde{w}}$, while microorganisms density, concentration, and the free stream nanofluid temperature are denoted by \bar{N}_{∞} , \bar{C}_{∞} , \bar{T}_{∞} , respectively.

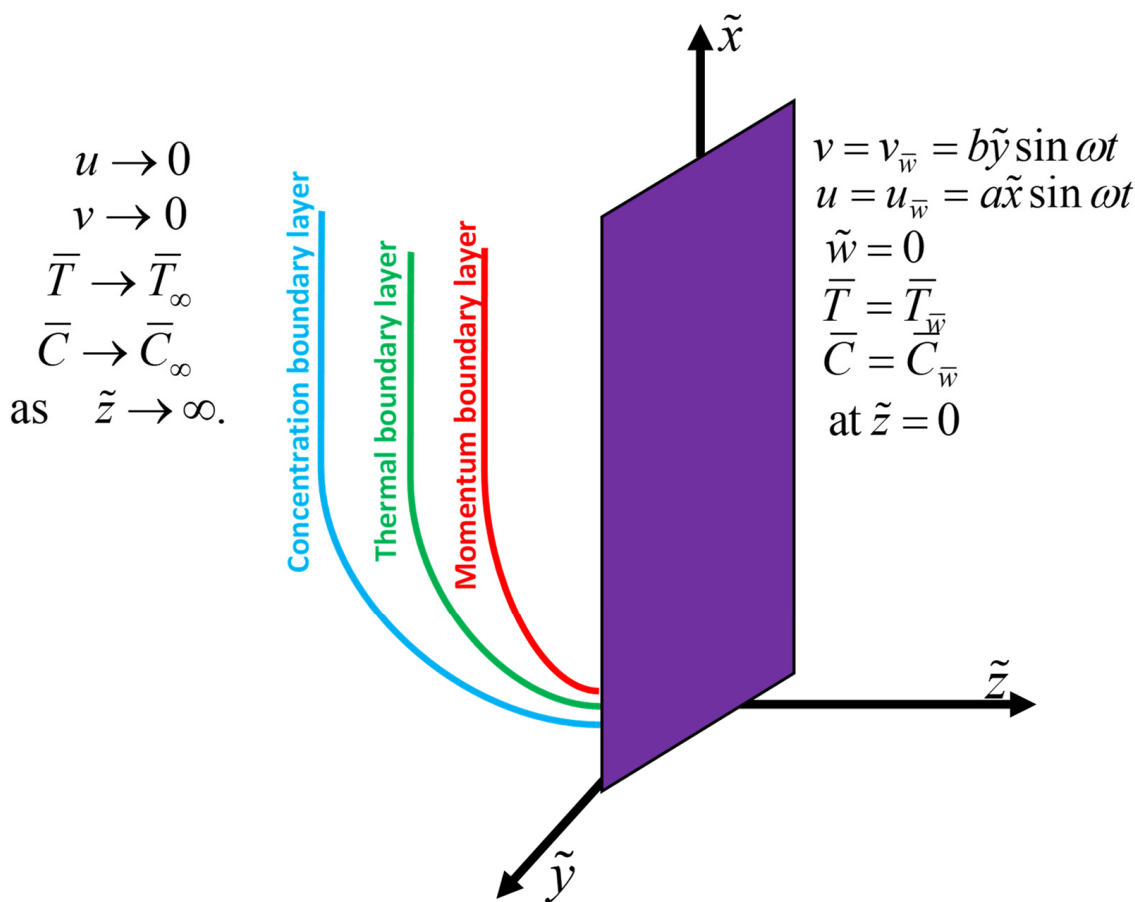


Figure 1. Flow geometry of the problem.

The resulting governing equations are presented as follows [30]:

$$\frac{\partial u}{\partial \tilde{x}} + \frac{\partial v}{\partial \tilde{y}} + \frac{\partial w}{\partial \tilde{z}} = 0,$$

$$\frac{\partial u}{\partial t} + u \left(\frac{\partial u}{\partial \tilde{x}} \right) + v \left(\frac{\partial u}{\partial \tilde{y}} \right) + w \left(\frac{\partial u}{\partial \tilde{z}} \right) = \frac{\nu}{(1+\Omega)} \left(\frac{\partial^2 u}{\partial \tilde{z}^2} \right) + \frac{\nu \alpha_*}{(1+\Omega)} \left(\begin{aligned} &\frac{\partial^3 u}{\partial \tilde{z}^2 \partial t} + v \frac{\partial^3 u}{\partial \tilde{y} \partial \tilde{z}^2} + w \frac{\partial^3 u}{\partial \tilde{z}^3} \\ &+ u \frac{\partial^3 u}{\partial \tilde{x} \partial \tilde{z}^2} + \left(\frac{\partial v}{\partial \tilde{z}} \right) \left(\frac{\partial^2 u}{\partial \tilde{y} \partial \tilde{z}} \right) \\ &+ \left(\frac{\partial u}{\partial \tilde{z}} \right) \left(\frac{\partial^2 u}{\partial \tilde{x} \partial \tilde{z}} \right) + \left(\frac{\partial w}{\partial \tilde{z}} \right) \left(\frac{\partial^2 u}{\partial \tilde{z}^2} \right) \end{aligned} \right) \tag{2}$$

$$- \frac{\nu u}{k_p} + \frac{g}{\rho_f} \left[\rho_f \varphi (1 - \bar{C}_\infty) (\bar{T} - \bar{T}_\infty) - (\rho_p - \rho_f) (\bar{C} - \bar{C}_\infty) - \sigma_* (\rho_m - \rho_f) (\bar{N} - \bar{N}_\infty) \right]$$

$$\frac{\partial v}{\partial t} + u \frac{\partial v}{\partial \tilde{x}} + v \frac{\partial v}{\partial \tilde{y}} + w \frac{\partial v}{\partial \tilde{z}} = \frac{\nu}{(1+\Omega)} \left(\frac{\partial^2 v}{\partial \tilde{z}^2} \right) + \frac{\nu \alpha_*}{(1+\Omega)} \left(\begin{aligned} &\frac{\partial^3 v}{\partial \tilde{z}^2 \partial t} + v \frac{\partial^3 v}{\partial \tilde{y} \partial \tilde{z}^2} + w \frac{\partial^3 v}{\partial \tilde{z}^3} \\ &+ \left(\frac{\partial u}{\partial \tilde{z}} \right) \left(\frac{\partial^2 v}{\partial \tilde{x} \partial \tilde{z}} \right) + u \frac{\partial^3 v}{\partial \tilde{x} \partial \tilde{z}^2} \\ &+ \left(\frac{\partial w}{\partial \tilde{z}} \right) \left(\frac{\partial^2 v}{\partial \tilde{z}^2} \right) + \left(\frac{\partial v}{\partial \tilde{z}} \right) \left(\frac{\partial^2 v}{\partial \tilde{y} \partial \tilde{z}} \right) \end{aligned} \right) - \frac{\nu u}{k_p}, \tag{3}$$

$$\frac{\partial \bar{T}}{\partial t} + u \frac{\partial \bar{T}}{\partial \tilde{x}} + v \frac{\partial \bar{T}}{\partial \tilde{y}} + w \frac{\partial \bar{T}}{\partial \tilde{z}} + \delta_{\bar{T}} \left[\begin{aligned} &2u \frac{\partial^2 \bar{T}}{\partial \tilde{x} \partial t} + w^2 \frac{\partial^2 \bar{T}}{\partial \tilde{z}^2} + v^2 \frac{\partial^2 \bar{T}}{\partial \tilde{y}^2} + u^2 \frac{\partial^2 \bar{T}}{\partial \tilde{x}^2} + 2w \frac{\partial^2 \bar{T}}{\partial \tilde{z} \partial t} + w \frac{\partial u}{\partial \tilde{z}} \frac{\partial \bar{T}}{\partial \tilde{x}} \\ &+ v \left(\frac{\partial v}{\partial \tilde{y}} \frac{\partial \bar{T}}{\partial \tilde{y}} + \frac{\partial w}{\partial \tilde{y}} \frac{\partial \bar{T}}{\partial \tilde{z}} \right) + u \left(\frac{\partial u}{\partial \tilde{x}} \frac{\partial \bar{T}}{\partial \tilde{x}} + \frac{\partial v}{\partial \tilde{x}} \frac{\partial \bar{T}}{\partial \tilde{y}} + \frac{\partial w}{\partial \tilde{x}} \frac{\partial \bar{T}}{\partial \tilde{z}} \right) \\ &+ \frac{\partial u}{\partial t} \frac{\partial \bar{T}}{\partial \tilde{x}} + \frac{\partial v}{\partial t} \frac{\partial \bar{T}}{\partial \tilde{y}} + \frac{\partial w}{\partial t} \frac{\partial \bar{T}}{\partial \tilde{z}} + \frac{\partial^2 \bar{T}}{\partial t^2} + v \frac{\partial u}{\partial \tilde{y}} \frac{\partial \bar{T}}{\partial \tilde{x}} + w \frac{\partial v}{\partial \tilde{z}} \frac{\partial \bar{T}}{\partial \tilde{y}} \\ &+ 2v \left(u \frac{\partial^2 \bar{T}}{\partial \tilde{x} \partial \tilde{y}} + w \frac{\partial^2 \bar{T}}{\partial \tilde{y} \partial \tilde{z}} + \frac{\partial^2 \bar{T}}{\partial \tilde{y} \partial t} \right) + w \left(2u \frac{\partial^2 \bar{T}}{\partial \tilde{x} \partial \tilde{z}} + \frac{\partial w}{\partial \tilde{z}} \frac{\partial \bar{T}}{\partial \tilde{z}} \right) \end{aligned} \right] \tag{4}$$

$$= \frac{1}{(\rho c)_f} \frac{\partial}{\partial \tilde{z}} \left(k(\bar{T}) \frac{\partial \bar{T}}{\partial \tilde{z}} \right) + \frac{16 T_\infty^3 \sigma_r}{3(\rho c)_f k_r} \frac{\partial^2 \bar{T}}{\partial \tilde{y}^2} + U \left(D_B \frac{\partial \bar{C}}{\partial \tilde{z}} \frac{\partial \bar{T}}{\partial \tilde{z}} + \left(\frac{\partial \bar{T}}{\partial \tilde{z}} \right)^2 \frac{D_T}{T_\infty} \right),$$

$$\frac{\partial \bar{C}}{\partial t} + u \frac{\partial \bar{C}}{\partial x} + v \frac{\partial \bar{C}}{\partial y} + w \frac{\partial \bar{C}}{\partial z} + \delta_{\bar{C}} \left[\begin{aligned} & 2u \frac{\partial^2 \bar{C}}{\partial x \partial t} + w^2 \frac{\partial^2 \bar{C}}{\partial z^2} + v^2 \frac{\partial^2 \bar{C}}{\partial y^2} + u^2 \frac{\partial^2 \bar{C}}{\partial x^2} + 2w \frac{\partial^2 \bar{C}}{\partial z \partial t} + w \frac{\partial u}{\partial z} \frac{\partial \bar{C}}{\partial x} \\ & + v \frac{\partial v}{\partial y} \frac{\partial \bar{C}}{\partial y} + u \left(\frac{\partial u}{\partial x} \frac{\partial \bar{C}}{\partial x} + \frac{\partial v}{\partial x} \frac{\partial \bar{C}}{\partial y} + \frac{\partial w}{\partial x} \frac{\partial \bar{C}}{\partial z} \right) + v \frac{\partial w}{\partial y} \frac{\partial \bar{C}}{\partial z} \\ & + \frac{\partial u}{\partial t} \frac{\partial \bar{C}}{\partial x} + \frac{\partial v}{\partial t} \frac{\partial \bar{C}}{\partial y} + \frac{\partial w}{\partial t} \frac{\partial \bar{C}}{\partial z} + \frac{\partial^2 \bar{C}}{\partial t^2} + v \frac{\partial u}{\partial y} \frac{\partial \bar{C}}{\partial x} + w \frac{\partial v}{\partial z} \frac{\partial \bar{C}}{\partial y} \\ & + 2v \left(u \frac{\partial^2 \bar{C}}{\partial x \partial y} + w \frac{\partial^2 \bar{C}}{\partial y \partial z} + \frac{\partial^2 \bar{C}}{\partial y \partial t} \right) + w \left(2u \frac{\partial^2 \bar{C}}{\partial x \partial z} + \frac{\partial w}{\partial z} \frac{\partial \bar{C}}{\partial z} \right) \end{aligned} \right] \tag{5}$$

$$= D_{\bar{B}} \frac{\partial^2 \bar{C}}{\partial z^2} + \left(\frac{D_{\bar{T}}}{T_{\infty}} \right) \frac{\partial^2 \bar{T}}{\partial z^2} - K_r^2 (\bar{C} - \bar{C}_{\infty}) \left(\frac{\bar{T}}{T_{\infty}} \right)^m \exp \left(\frac{-E_{\circ}}{\beta_{\circ} \bar{T}} \right).$$

$$\frac{\partial \bar{N}}{\partial t} + u \frac{\partial \bar{N}}{\partial x} + v \frac{\partial \bar{N}}{\partial y} + w \frac{\partial \bar{N}}{\partial z} + \frac{\Re \Im}{(\bar{C}_{\bar{w}} - \bar{C}_{\infty})} \left[\frac{\partial}{\partial z} \left(\bar{N} \frac{\partial \bar{C}}{\partial z} \right) \right] = D_{\bar{m}} \frac{\partial^2 \bar{N}}{\partial z^2}. \tag{6}$$

With appropriate boundary constraints [21]:

$$\left. \begin{aligned} U_{\bar{w}} &= a\tilde{x} \sin \omega t, \quad v = / \\ u &\rightarrow 0, \quad \frac{\partial u}{\partial \tilde{z}} \rightarrow 0, \quad v \rightarrow 0, \quad \frac{\partial v}{\partial \tilde{z}} \rightarrow 0, \quad \bar{T} \rightarrow \bar{T}_{\infty}, \quad \bar{C} \rightarrow \bar{C}_{\infty}, \quad \bar{N} \rightarrow \bar{N}_{\infty}, \quad \text{as } \tilde{z} \rightarrow \infty. \end{aligned} \right\} \tag{7}$$

With, $\Omega, \nu, k_p, \alpha_*, g, \delta_{\bar{T}}, \wp, \sigma_*, \sigma_r, k_r, k(\bar{T}), \bar{U} = \left(\frac{\rho c}{\rho c} \right)_{\bar{n}}^{\bar{f}}, K, \delta_{\bar{C}}, m, \beta_{\circ}, E_{\circ}, \Re, \Im, \left(\rho_{\bar{p}}, \rho_{\bar{m}}, \rho_{\bar{f}} \right)$ and $(D_{\bar{T}}, D_{\bar{B}}, D_{\bar{m}})$ represent the ratio of relaxation and delay times; kinematic viscosity; porous medium permeability; retardation time; the gravitational acceleration; thermal relaxation time; thermal expansion coefficient; the microorganisms volume; Stefan Boltzmann constant; Boltzmann constant; thermal conductivity; the heat capacities ratio; reaction rate; solutal relaxation time; the rate constant; activation energy; chemotaxis constant; the swimming cell speed; densities for the nanoparticles, microorganisms, and the base fluid; and diffusivities for thermophoresis, Brownian, and microorganisms, respectively.

In addition, $k(\bar{T})$ is expressed as

$$k(\bar{T}) = k_{\infty}(1 + \varepsilon\theta), \tag{8}$$

where ε is a small parameter, k_{∞} is the thermal conductivity at the ambient zone, and θ is the dimensionless temperature.

To obtain the dimensionless expressions, the associated transformations are [21]

$$\left. \begin{aligned} u &= a\tilde{x}f_{\xi}(\xi, \tau), \quad w = -\sqrt{\nu a}[f(\xi, \tau) + g(\xi, \tau)], \quad v = a\tilde{y}g_{\xi}(\xi, \tau) \quad \tau = t\omega, \\ \xi &= \sqrt{\frac{a}{\nu}}\tilde{z}, \quad \phi(\xi, \tau) = \frac{\bar{C} - \bar{C}_{\infty}}{\bar{C}_{\bar{w}} - \bar{C}_{\infty}}, \quad \theta(\xi, \tau) = \frac{\bar{T} - \bar{T}_{\infty}}{\bar{T}_{\bar{w}} - \bar{T}_{\infty}}, \quad \chi(\xi, \tau) = \frac{\bar{N} - \bar{N}_{\infty}}{\bar{N}_{\bar{w}} - \bar{N}_{\infty}}. \end{aligned} \right\} \tag{9}$$

The dimensionless system is

$$f_{\xi\xi\xi} - (1 + \Omega)(f_{\xi}^2 + Sf_{\xi\tau} - (f + g)f_{\xi\xi} + \gamma f_{\xi}) + \Psi \left(\begin{aligned} & Sf_{\xi\xi\xi\tau} - (g + f)f_{\xi\xi\xi\xi} \\ & + f_{\xi\xi}^2 - g_{\xi}f_{\xi\xi\xi} \end{aligned} \right) + (1 + \Omega)(\omega\theta - \omega N\phi - \omega \Pi\chi) = 0, \tag{10}$$

$$g_{\xi\xi\xi} - (1 + \Omega)(g_{\xi}^2 + Sg_{\xi\tau} - (f + g)g_{\xi\xi} + \gamma g_{\xi}) + \Psi \left(\begin{aligned} & Sg_{\xi\xi\xi\tau} - (g + f)g_{\xi\xi\xi\xi} \\ & + g_{\xi\xi}^2 - f_{\xi}g_{\xi\xi\xi} \end{aligned} \right) = 0, \tag{11}$$

$$\left(\frac{1 + Rd}{Pr} \right) [(1 + \varepsilon\theta)\theta_{\xi\xi} + \varepsilon\theta_{\xi}^2] + Pr \left(\begin{aligned} & g\theta_{\xi} + f\theta_{\xi} - S\theta_{\tau} + N_t\theta_{\xi}^2 \\ & + N_b\theta_{\xi}\phi_{\xi} \end{aligned} \right) - Pr\delta_1 \left(\begin{aligned} & S^2\theta_{\tau\tau} - S(f_{\tau}\theta_{\xi} + g_{\tau}\theta_{\xi}) \\ & - 2S(g + f)\theta_{\tau\xi} + (g + f)^2\theta_{\xi\xi} \\ & + (f_{\xi} + g_{\xi})(f + g)\theta_{\xi} \end{aligned} \right) = 0, \tag{12}$$

$$\phi_{\xi\bar{\xi}} + Sc(g\phi_{\xi} + f\phi_{\bar{\xi}} - S\phi_{\tau}) - Sc\delta_2 \left(\begin{matrix} S^2\phi_{\tau\tau} - S(f_{\tau}\phi_{\xi} + g_{\tau}\phi_{\bar{\xi}}) \\ -2S(g+f)\phi_{\tau\xi} + (g+f)^2\phi_{\xi\xi} \\ + (f_{\xi} + g_{\bar{\xi}})(f+g)\phi_{\xi} \end{matrix} \right) + \frac{N_t}{N_b}\theta_{\xi\bar{\xi}} - Sc\Delta(1 + \Lambda\theta)^m \phi \exp\left(-\frac{\Theta}{1+\Lambda\theta}\right) = 0, \tag{13}$$

$$\chi_{\xi\bar{\xi}} + \Upsilon(g\chi_{\xi} + f\chi_{\bar{\xi}} - S\chi_{\tau}) - \beta((\chi + \Gamma)\phi_{\xi\bar{\xi}} + \chi_{\xi}\phi_{\bar{\xi}}) = 0. \tag{14}$$

With the boundary conditions:

$$\left. \begin{matrix} f_{\xi}(0, \tau) = \sin \tau, & f(0, \tau) = 0, & g_{\bar{\xi}}(0, \tau) = A \sin \tau, & g(0, \tau) = 0, \\ g_{\xi}(\infty, \tau) = 0, & f_{\xi}(\infty, \tau) = 0, & g_{\xi\bar{\xi}}(\infty, \tau) = 0, & f_{\xi\bar{\xi}}(\infty, \tau) = 0, & \chi(0, \tau) = 1, \\ \theta(0, \tau) = 1, & \phi(0, \tau) = 1, & \chi(\infty, \tau) = 0, & \theta(\infty, \tau) = 0 & \phi(\infty, \tau) = 0. \end{matrix} \right\} \tag{15}$$

The physical parameters Ψ (Deborah number), N (buoyancy ratio parameter), ω (mixed convection parameter), Pr (Prandtl number), Π (bioconvective Rayleigh number), N_b (Brownian motion parameter), Rd (radiation parameter), N_t (thermophoresis parameter), δ_1 (thermic relaxation constant), Sc (Schmidt number), S (angular frequency to stretching rate ratio), δ_2 (solutal relaxation), Υ (bioconvective Lewis number), γ (porosity parameter), Δ (reaction rate), β (bioconvective Peclet number), Λ (temperature difference), Γ (concentration difference constant for microorganisms), A (stretching ratio), and Θ (activation energy) are defined as follows:

$$\left. \begin{matrix} S = \frac{\omega}{a}, & \omega = \frac{\varphi g(1-\bar{C}_{\infty})(\bar{T}_w - \bar{T}_{\infty})}{a^2 \bar{\chi}}, & N = \frac{(\rho_p - \rho_f)(\bar{C}_w - \bar{C}_{\infty})}{\rho_f \varphi(1-\bar{C}_{\infty})(\bar{T}_w - \bar{T}_{\infty})}, & \gamma = \frac{\nu}{ak_p}, & R = 16\sigma_r T_{\infty}^3 / 3k_r k, \\ \Psi = \alpha_* a, & \Pi = \frac{\sigma_* (\rho_m - \rho_f)(\bar{N}_w - \bar{N}_{\infty})}{\rho_f \varphi(1-\bar{C}_{\infty})(\bar{T}_w - \bar{T}_{\infty})}, & \delta_1 = \delta_T a, & Sc = \frac{\nu}{D_B}, & \delta_2 = \delta_C a, \\ Y = \frac{\nu}{D_m}, & \Delta = \frac{K_r^2}{a}, & \beta = \frac{\Re S}{D_m}, & A = \frac{b}{a}, & N_b = \frac{\Upsilon D_B (\bar{C}_w - \bar{C}_{\infty})}{\nu}, & \Lambda = \frac{(\bar{T}_w - \bar{T}_{\infty})}{\bar{T}_{\infty}}, \\ N_t = \frac{\Upsilon D_T (\bar{T}_w - \bar{T}_{\infty})}{\nu \bar{T}_{\infty}}, & Pr = \frac{\mu c_p}{k_{\infty}}, & \Gamma = \frac{\bar{N}_{\infty}}{\bar{N}_w - \bar{N}_{\infty}}, & \Theta = \frac{E_{\circ}}{\beta_{\circ} \bar{T}_{\infty}}. \end{matrix} \right\} \tag{16}$$

The interesting physical quantities: local motile density ($Nn_{\bar{x}}$), local Nusselt number ($Nu_{\bar{x}}$), and local Sherwood ($Sh_{\bar{x}}$) are defined as

$$Nn_{\bar{x}} = \frac{\tilde{\chi}_{\xi}}{D_m(\bar{N}_w - \bar{N}_{\infty})}, \quad Nu_{\bar{x}} = \frac{\tilde{\chi}_{\diamond}}{k(\bar{T}_w - \bar{T}_{\infty})}, \quad Sh_{\bar{x}} = \frac{\tilde{\chi}_{\lambda}}{D_B(\bar{C}_w - \bar{C}_{\infty})}, \tag{17}$$

The mass, motile microorganisms, and heat surface fluxes (λ, ζ, \diamond) are expressed as

$$\lambda = -D_B \left(\frac{\partial \bar{C}}{\partial \bar{z}} \right)_{\bar{z}=0}, \quad \zeta = -D_m \left(\frac{\partial \bar{N}}{\partial \bar{z}} \right)_{\bar{z}=0}, \quad \diamond = -k \left(\frac{\partial \bar{T}}{\partial \bar{z}} \right)_{\bar{z}=0}. \tag{18}$$

By considering the dimensionless variables (Equation (8)), Equation (17) becomes

$$Nu_{\bar{x}} = -\left(1 + \frac{4}{3}Rd\right)\theta_{\xi}(0, \tau)\sqrt{Re_{\bar{x}}}, \quad Nn_{\bar{x}} = -\chi_{\xi}(0, \tau)\sqrt{Re_{\bar{x}}}, \quad Sh_{\bar{x}} = -\phi_{\xi}(0, \tau)\sqrt{Re_{\bar{x}}}. \tag{19}$$

With $Re_{\bar{x}} = \frac{U_w \tilde{x}}{\nu}$ the local Reynold's number.

3. Homotopy Analysis Method

The set of dimensionless partial differential governing equations is very complex. Thus, the analytical solution of these equations is obtained by using the homotopy analysis method (HAM). The HAM method is one of the best semi-analytical methods that can

be used to find solutions with excellent accuracy. This method, unlike the perturbation technique, does not impose any smaller parameter constraints. The flow chart of HAM method is presented in Figure 2. The method was proposed by Liao [31], and later, different studies are performed by using this method [32–34].



Figure 2. Flow chart of HAM method.

The initial guesses for the current flow problem are

$$\left. \begin{aligned} f_0(\zeta, \tau) &= \sin \tau(1 - \exp(-\zeta)), \theta_0(\zeta, \tau) = \exp(-\zeta), \chi_0(\zeta, \tau) = \exp(-\zeta), \\ g_0(\zeta, \tau) &= A \sin \tau(1 - \exp(-\zeta)), \phi_0(\zeta, \tau) = \exp(-\zeta). \end{aligned} \right\} \quad (20)$$

The linear auxiliary operators are

$$L_f = \frac{\partial^3}{\partial \zeta^3} - \frac{\partial}{\partial \zeta}, \quad L_g = \frac{\partial^3}{\partial \zeta^3} - \frac{\partial}{\partial \zeta}, \quad L_\theta = \frac{\partial^2}{\partial \zeta^2} - 1, \quad L_\phi = \frac{\partial^2}{\partial \zeta^2} - 1, \quad L_\chi = \frac{\partial^2}{\partial \zeta^2} - 1. \quad (21)$$

Fulfilling

$$\left. \begin{aligned} L_f \left(\sum_{k=0}^2 \mathbb{Z}_{k+1} e^{(k-1)\xi} \right) = 0, \quad L_g \left(\sum_{j=3}^5 \mathbb{Z}_{k+1} e^{(k-4)\xi} \right) = 0, \quad L_\theta \left(\sum_{j=6}^7 \mathbb{Z}_{k+1} e^{(-1)^k \xi} \right) = 0, \\ L_\phi \left(\sum_{k=8}^9 \mathbb{Z}_{k+1} e^{(-1)^k \xi} \right) = 0, \quad L_\chi \left(\sum_{k=10}^{11} \mathbb{Z}_{k+1} e^{(-1)^k \xi} \right) = 0, \end{aligned} \right\} \quad (22)$$

With $\mathbb{Z}_j (j = 1, 2, \dots, 12)$ being arbitrary constants. The analytic homotopic solution primarily depends on supplementary parameters $(h_\phi, h_\theta, h_\chi, h_f, h_g)$, and by giving accurate values to these parameters, the convergence can be reached. The region of convergence can be indicated by plotting h -curve which is shown in Figure 3. The choice of auxiliary parameters should be feasible for $-1.2 \leq h_f \leq -0.2$, $-1.8 \leq h_g \leq -0.2$, $-1.3 \leq h_\theta \leq -0.2$, $-1 \leq h_\phi \leq -0.05$, and $-1.2 \leq h_\chi \leq -0.4$.

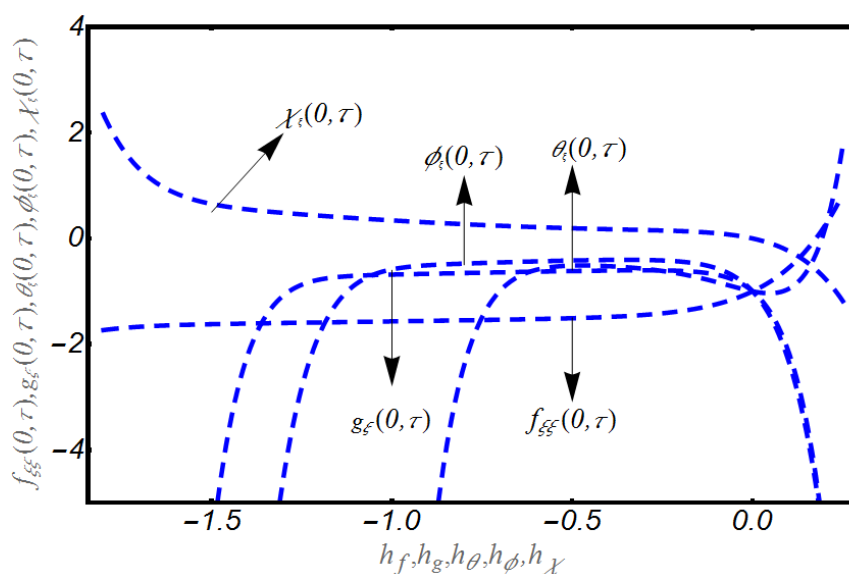


Figure 3. Curves for $f, \theta, \phi,$ and χ .

4. Verification of the Analytical Model

To check the validity of the current model, a comparison with the results of Ariel [27] is performed. As presented in Table 1, an excellent agreement between the results is encountered. It is to be mentioned that Ariel [35] studied the problem using the homotopy perturbation method.

Table 1. Comparison of analytical findings with those of Ariel [35] for $S = \Omega = \omega = \Pi = \gamma = 0$.

	Ariel [35]		Present Results	
A	$-f''(0)$	$-g''(0)$	$-f''(0)$	$-g''(0)$
0.0	1.00000	0.00000	1.00000	0.00000
0.1	1.02025	0.06684	1.020256	0.066856
0.2	1.03949	0.14873	1.039501	0.148719

5. Discussion

In this section, the velocity (f_ξ, g_ξ) , temperature θ , concentration ϕ , and microorganisms χ profiles are presented and discussed. The studied model is based on theoretical flow assumptions and the following parameters have been fixed as $\Omega = 0.2, S = 0.2, \Psi = 0.4, N_b = 0.3, \omega = 0.2, N_t = 0.3, Pr = 2, \Pi = 0.4, N = 0.4, Pr = 1.5, \gamma = 0.2, \gamma = 0.5, \delta_1 = 0.1, \varepsilon = 0.2, Sc = 0.4, \delta_2 = 0.3, \Delta = 0.3, \Upsilon = 0.7, \Lambda = 0.1, \beta = 0.7, \Theta = 0.2, \Gamma = 0.4,$ and $m = 0.4$. Figure 4a shows the effects of the Deborah number Ψ on the velocity field f_ξ . It is

seen that the velocity f_{ξ} obtains increasing variations for the rising values of Ψ . Physically, such observations are due to relaxation time features. Figure 4b is sketched to represent the behavior of f_{ξ} against different impacts of the oscillating frequency to the stretching rate S . The increasing of S causes a reduction in f_{ξ} . Moreover, a minor phase shift is also noticed for higher values of S . Figure 4c presents the effects of the porosity parameter γ on f_{ξ} . A decrease in the velocity oscillations occurs when γ is increased. Such observations are physically associated to the permeability of the porous media.

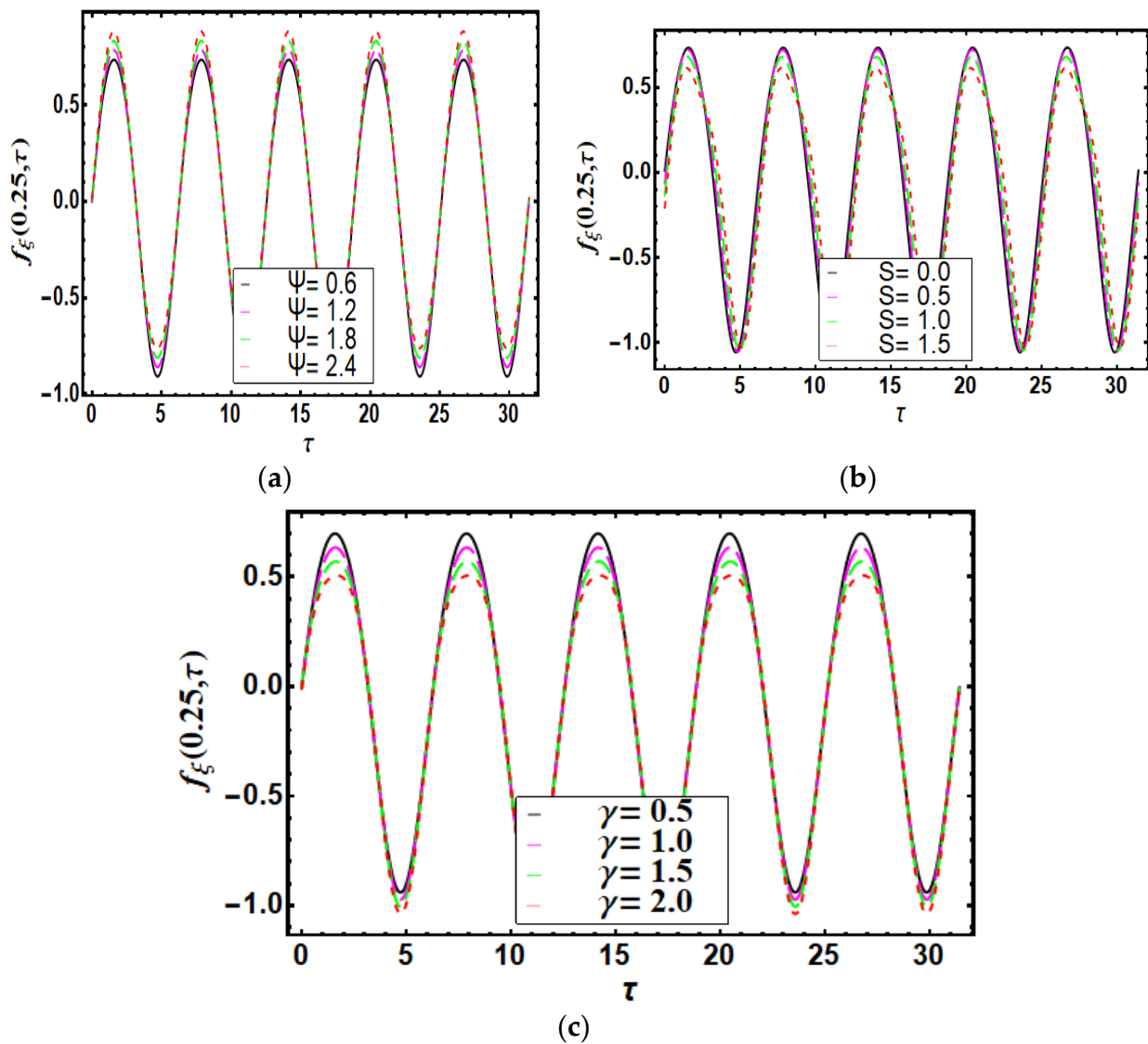


Figure 4. (a) Effects of Ψ on f_{ξ} . (b) Effects of S on f_{ξ} . (c) Effects of γ on f_{ξ} .

Figure 5a is plotted to analyze the effect of Ψ on the velocity profile g_{ξ} . An increase in the oscillation amplitude of the velocity is encountered when Ψ is increased. Figure 5b depicts the variation in the velocity g_{ξ} for different values of S . A reducing nature of the velocity is observed when larger S values are imposed. Such observations are associated to the oscillating frequency. Figure 5c is drawn to describe the behavior of g_{ξ} for various values of γ . A declining trend of the velocity amplitude is noticed when γ is increased. Such declining behavior is due to the permeability of porous media.

Figure 6a describes the temporal variations in the temperature for various values of Ψ . The temperature θ decreases with an increasing value of Ψ . Figure 6b presents the temperature variations for different values of the permeability parameter γ . The increase in γ leads to an augmentation of the temperature. Figure 6c is plotted to demonstrate the

behavior of the temperature profile θ when the thermic relaxation constant δ_1 is varied. A considerable increase in the temperature occurs for higher values of δ_1 .

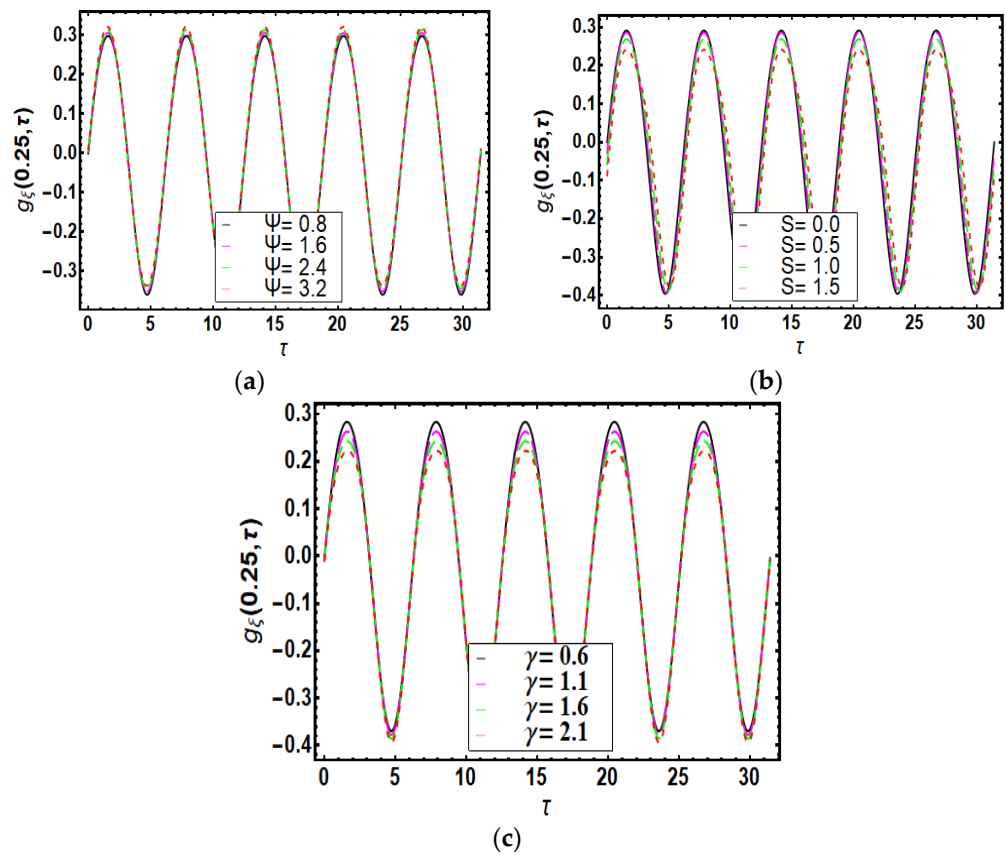


Figure 5. (a) Effects of Ψ on g_ζ . (b) Effects of S on g_ζ . (c) Effects of γ on g_ζ .

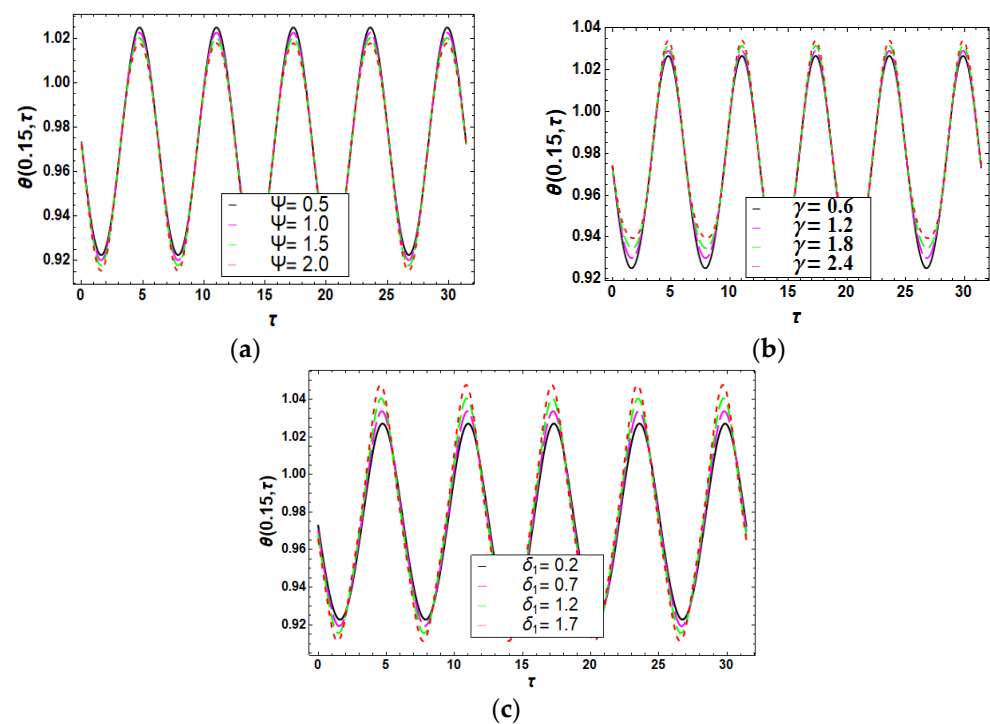


Figure 6. (a) Effects of Ψ on θ . (b) Effects of γ on θ . (c) Effects of δ_1 on θ .

Figure 7a shows the influence of Ψ on the concentration profile ϕ . A reduction in the concentration amplitude occurs when Ψ is increased. Figure 7b presents the concentration variations ϕ for different solutal relaxation δ_2 values. It is shown that the increase in δ_2 causes an increase in the concentration. Figure 8a shows the variation in the motile microorganisms χ for various Ψ (Deborah number) values. It is noticed that the increase in Ψ causes the increase in the motile microorganisms' values. Figure 8b presents the behavior of the motile microorganisms χ for different values of γ . It is seen that the motile microorganisms are higher for higher values of γ .

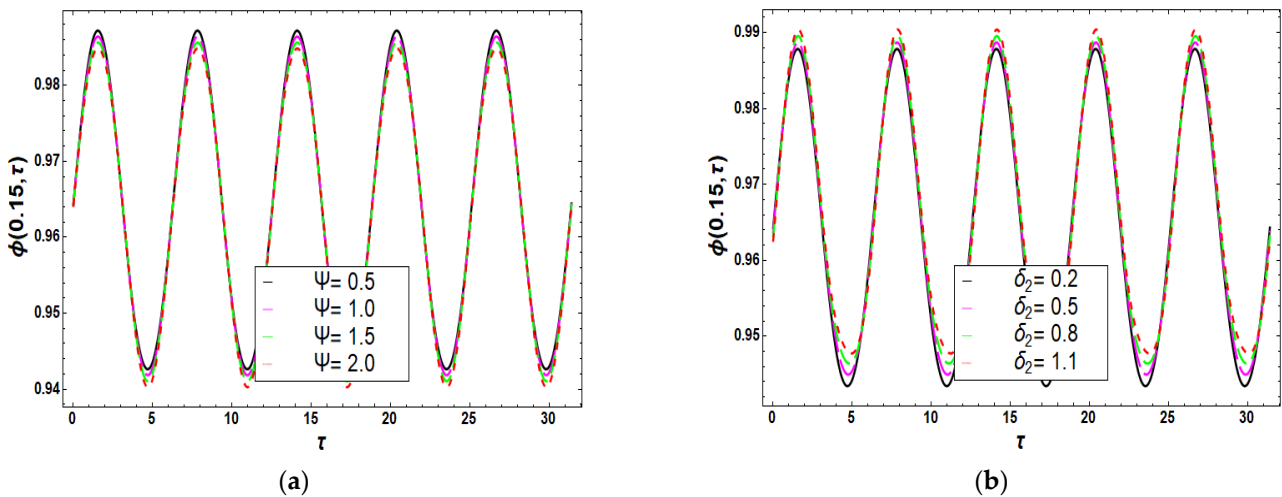


Figure 7. (a) Effects of Ψ on ϕ . (b) Effects of δ_2 on ϕ .

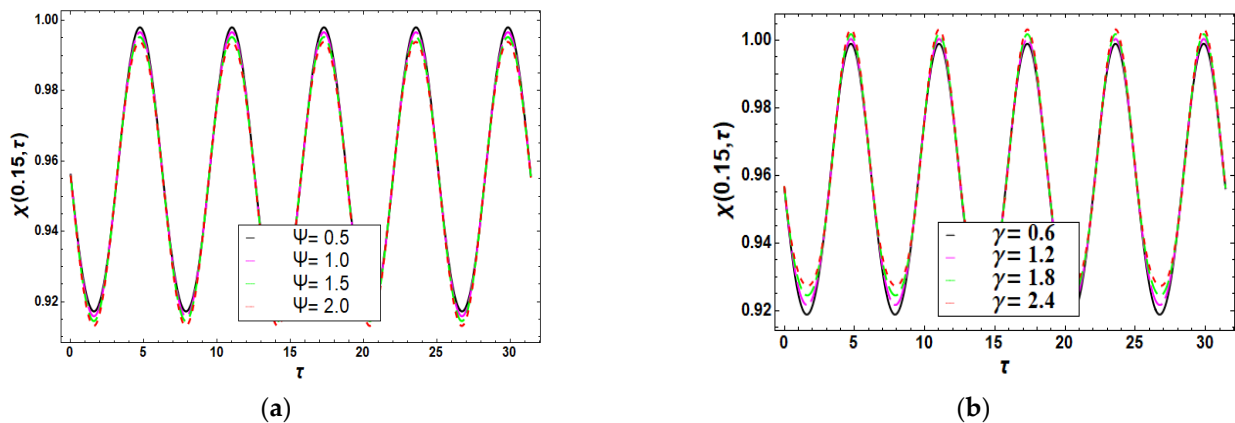


Figure 8. (a) Effects of ψ on χ . (b) Effects of γ on χ .

Figure 9 presents the velocity profile f_{ξ} for various porosity parameter γ and mixed convection parameter ω . It is noticed that the velocity increases with ω , while the opposite occurs for γ . Figure 10 is sketched to show the profile of g_{ξ} for different values of the bioconvective Rayleigh number Π and buoyancy ratio N . The increases in the Rayleigh number and buoyancy ratio lead to the intensification of the flow due to the density variation and thus cause the increase in the velocity.

Figure 11 depicts the impact of the radiation parameter Rd and thermal conductivity parameter ϵ on the temperature profile θ . Both of these parameters have a beneficial effect of the temperature increasing. The augmentation of the temperature due to Rd is associated to the electromagnetic waves. The thermal radiation effects are important in enhancing the heat transfer rate and have several applications in solar management systems. The increase in the thermal conductivity leads to an enhancement of the heat transfer rate and consequently an increase in the temperature. In Figure 12, the observations are predicted for

θ due to the Brownian motion parameter N_b and the ratio of the oscillating frequency to the stretched rate S . A larger thermal contribution of θ for larger N_b is exhibited. Physically, the increasing heat transfer rate is due to the random motion of tiny particles. The enhancement in θ for S is due to a larger oscillating frequency.

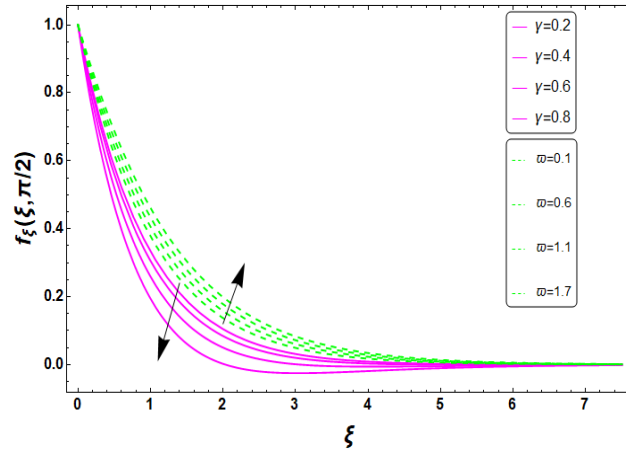


Figure 9. Profile of f_{ξ} for various values of γ and ω .

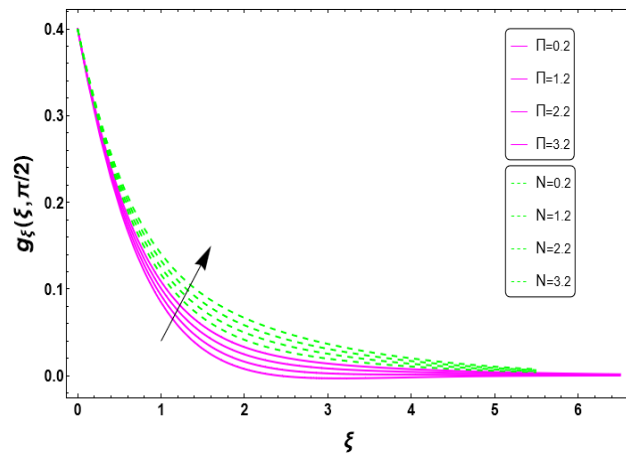


Figure 10. Profile of g_{ξ} for various values Π and N .

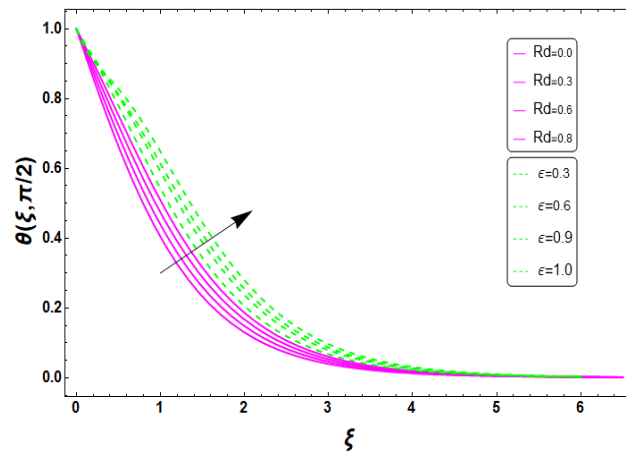


Figure 11. Profile of θ for various values of Rd and ϵ .

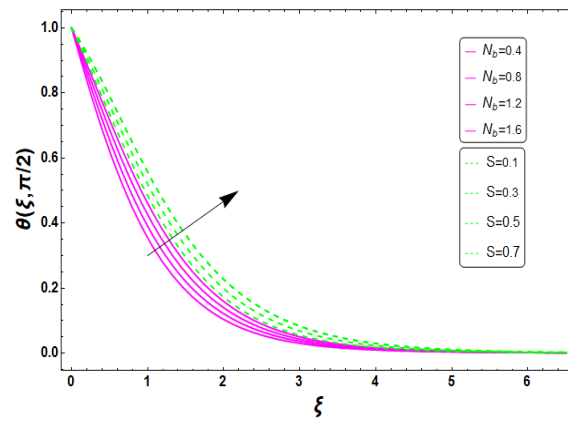


Figure 12. Profile of θ for various values of N_b and S .

Figure 13 is plotted to depict the profiles of ϕ for different values of the thermophoresis parameter N_t and activation energy factor Θ . An improvement in the concentration profile is noticed due to the increase in N_t and Θ . The thermophoresis phenomenon is caused by the motions of the tiny particles from the hot region toward the cold surface. This migration reveals an enhancement in the concentration pattern of the tiny particles. Due to the intensification of the chemical process, the increase in concentration occurs also when the activation energy parameter is increased. Figure 14 demonstrates the behavior of the concentration profile ϕ caused by the variation in the reaction rate Δ and temperature difference parameter Λ values. It can be concluded that for larger Δ and Λ values, a decrease in concentration ϕ is noticed. Figure 15 presents the variations in ϕ for different values of the Schmidt number Sc and solutal relaxation δ_2 . Lower values of ϕ are encountered with the increase in Sc . Physically, such observations are due to the smaller mass diffusivities. Similar observations can be mentioned for the effect of solutal relaxation δ_2 . Figure 16 shows the motile microorganisms' profiles χ for various values of β (bioconvective Peclet number) and Υ (bioconvective Lewis number). It is clear that when the values of β and Υ increase, they cause a reduction in the motile microorganisms' values χ . Figure 17 shows the profiles of χ for different values of the Peclet Pe and bioconvective Lewis numbers Lb . A reduction in χ is noticed for lower Pe and Lb values. This reduction is associated to the low motile densities. Figure 18 is plotted to show the behavior of motile microorganisms caused by the change in the Γ (concentration difference constant for microorganisms) and γ (porosity parameter) values. The microorganism's concentration is enhanced with higher Γ values but decreases with γ . Table 2 presents the computed outcomes of $Nu_{\bar{x}}(Re_{\bar{x}})^{-0.5}$, $Sh_{\bar{x}}(Re_{\bar{x}})^{-0.5}$, and $Nn_{\bar{x}}(Re_{\bar{x}})^{-0.5}$ for several values of the governing parameters. Smaller values of these physical quantities occur for higher values of Ω , γ , and ε .

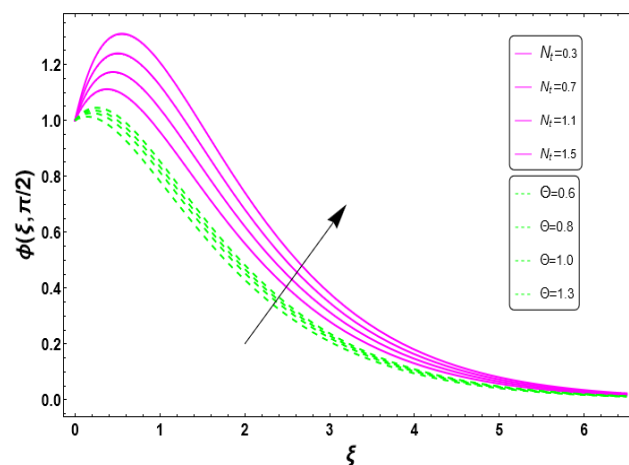


Figure 13. Profile of ϕ for N_t and Θ .

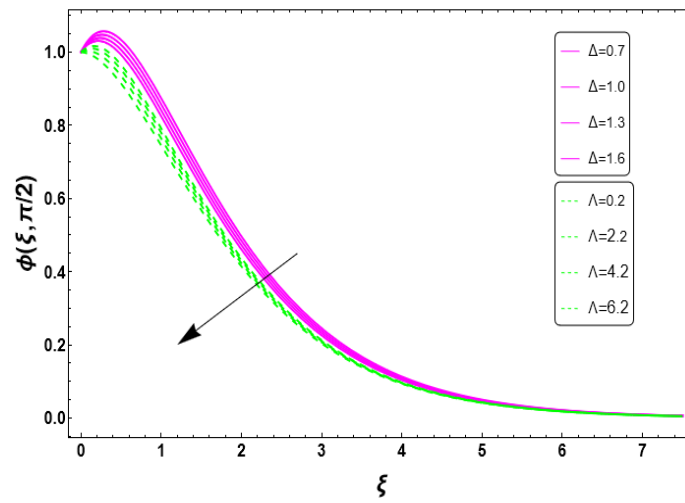


Figure 14. Profile of ϕ for Δ and Λ .

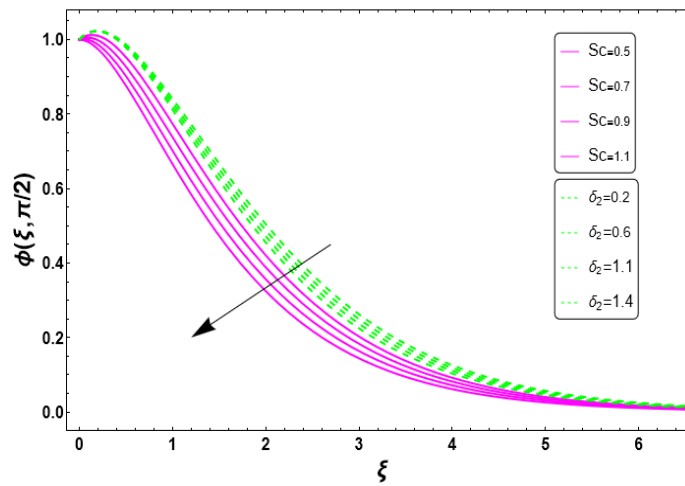


Figure 15. Profile of ϕ for Sc and δ_2 .

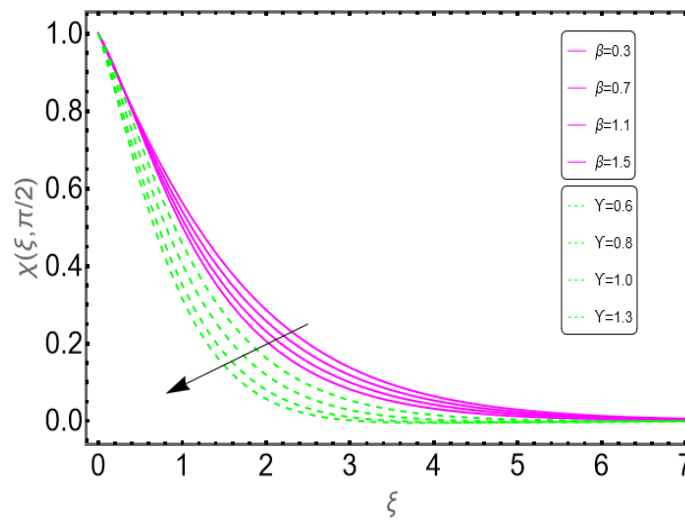


Figure 16. Profile of χ for β and γ .

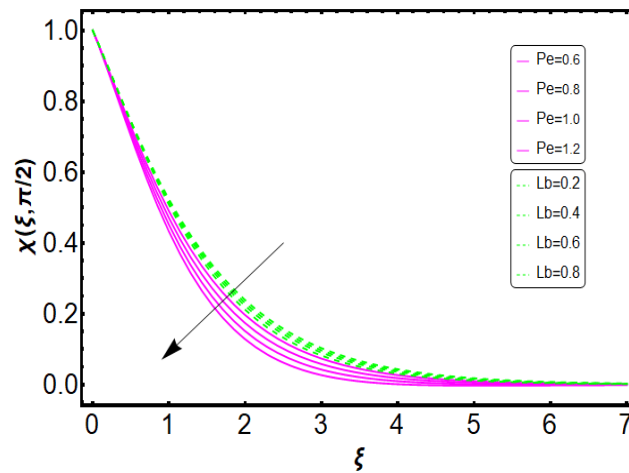


Figure 17. Profile of χ for Pe and Lb .

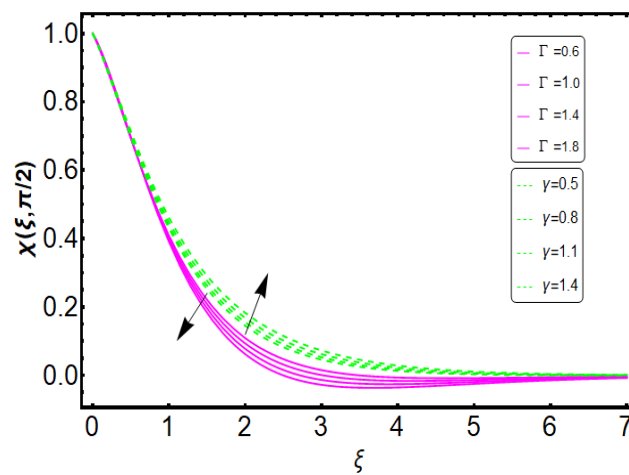


Figure 18. Profile of χ for Γ and γ .

Table 2. Physical implications of parameters for $Nu_{\bar{x}}(Re_{\bar{x}})^{-0.5}$, $Sh_{\bar{x}}(Re_{\bar{x}})^{-0.5}$, and $Nn_{\bar{x}}(Re_{\bar{x}})^{-0.5}$.

Ω	Ψ	Pr	δ_1	ϵ	γ	$Nu_{\bar{x}}(Re_{\bar{x}})^{-0.5}$	$Sh_{\bar{x}}(Re_{\bar{x}})^{-0.5}$	$Nn_{\bar{x}}(Re_{\bar{x}})^{-0.5}$
0.4	0.2	1.5	0.3	0.2	0.4	0.5562	0.41537	0.5394
0.5						0.3857	0.5246	
0.6						0.3646	0.4942	
0.2	0.50					0.4404	0.38325	0.5131
						0.4724	0.3956	0.4823
						0.4968	0.43577	0.4634
		0.7				0.4505	0.4156	0.5332
		1.1				0.4877	0.43435	0.5554
		1.5				0.5143	0.4435	0.5635
			0.2			0.4403	0.45032	0.5642
			0.3			0.4654	0.46435	0.5847
			0.4			0.5153	0.4935	0.6242
				0.3		0.4345	0.40466	0.5035
				0.5		0.3965	0.38466	0.4842
				0.7		0.3546	0.37343	0.4435
					0.4	0.4832	0.49353	0.55456
					0.6	0.4353	0.43577	0.5246
					0.8	0.3868	0.41334	0.4756

6. Conclusions

The bioconvective Jeffrey fluid conveying tiny particles with variable thermal conductivity is studied. The mass and heat transfers are modeled using Cattaneo–Christov diffusion theories. The bidirectional porous oscillating surface induces the flow. The dimensionless system is solved via the homotopy analysis scheme. The convergence of the HAM scheme is ensured. The main findings can be summarized as follows:

- An increase in the amplitude of the velocity occurs for a higher Deborah number without any phase shift.
- A lower velocity magnitude is encountered for the porosity parameter.
- The temporal variation in the temperature time increases with the increase in the thermic relaxation constant and the porosity parameter.
- The impact of the Deborah number has been found to reduce the concentration and microorganisms' profiles.
- The temperature profiles have higher values for a higher radiation parameter and the ratio of the oscillating frequency to the stretched rate.
- The variable thermal conductivity assumptions are very effective in improving the heat transfer rate.
- The increase in the chemical reaction parameter, Lewis number, and solutal relaxation reduces the concentration profile.
- With the increment of the concentration difference constant, the microorganism profile has lower values.
- With an increasing porosity parameter, the microorganism profile is enhanced.
- The Local Nusselt number, Sherwood number, and motile density number are enhanced with the Prandtl number and thermic relaxation constant.

Author Contributions: Conceptualization, L.K., N.B.K. and S.U.K.; methodology, K.A.-K., L.K. and N.B.K.; software, S.U.K.; validation, S.U.K., L.K., and N.B.K.; formal analysis, L.K., N.B.K. and S.U.K.; investigation, K.A.-K., L.K. and N.B.K.; writing—original draft preparation, L.K., K.A.-K., N.B.K. and S.U.K.; writing—review and editing, L.K., K.A.-K., N.B.K. and S.U.K.; project administration, L.K.; funding acquisition, L.K. All authors have read and agreed to the published version of the manuscript.

Funding: This research has been funded by the Deputy for Research & Innovation, Ministry of Education, through the Initiative of Institutional Funding at University of Ha'il—Saudi Arabia through project number IFP-22 001.

Institutional Review Board Statement: Not applicable.

Informed Consent Statement: Not applicable.

Data Availability Statement: Not applicable.

Conflicts of Interest: The authors declare no conflict of interest.

References

1. Choi, S.U.S. Enhancing thermal conductivity of fluids with nanoparticles. *ASME-Publ. Fed.* **1995**, *231*, 99–106.
2. Buongiorno, J. Convective transport in nanofluids. *J. Heat Transf.* **2006**, *128*, 240–250. [[CrossRef](#)]
3. Mahmud, K.; Rana, S.; Al-Zubaidi, A.; Mehmood, R.; Saleem, S. Interaction of Lorentz force with cross swimming microbes in couple stress nano fluid past a porous Riga plate. *Int. Commun. Heat Mass Transf.* **2022**, *138*, 106347. [[CrossRef](#)]
4. Madkhali, H.A.; Haneef, M.; El-Shafay, A.S.; Alharbi, S.O.; Nawaz, M. Mixed convective transport in Maxwell hybrid nano-fluid under generalized Fourier and Fick laws. *Int. Commun. Heat Mass Transf.* **2022**, *130*, 105714. [[CrossRef](#)]
5. Hameed, N.; Noeiaghdam, S.; Khan, W.; Pimpunchat, B.; Fernandez-Gamiz, U.; Khan, M.S.; Rehman, A. Analytical analysis of the magnetic field, heat generation and absorption, viscous dissipation on couple stress casson hybrid nano fluid over a nonlinear stretching surface. *Results Eng.* **2022**, *16*, 100601. [[CrossRef](#)]
6. Chandrasekaran, M.; Prakash, K.B.; Subramaniyan, C.; Santhosh, N.; Tamilarasan, V.D. Experimental investigation on heavy duty engine radiator using cerium oxide nano fluid. *Mater. Today Proc.* **2022**, *66*, 1497–1500. [[CrossRef](#)]

7. Cui, J.; Razzaq, R.; Farooq, U.; Khan, W.A.; Farooq, F.B.; Muhammad, T. Impact of non-similar modeling for forced convection analysis of nano-fluid flow over stretching sheet with chemical reaction and heat generation. *Alex. Eng. J.* **2022**, *61*, 4253–4261. [[CrossRef](#)]
8. Mishra, G.; Chhabra, R.P. Effects of flow fluctuations and buoyancy on heat transfer from a sphere in non-Newtonian nano fluids: Potential for intensification. *Chem. Eng. Process. Process Intensif.* **2022**, *178*, 109048. [[CrossRef](#)]
9. Mahmud, K.; Mehmood, R.; Rana, S.; Al-Zubaidi, A. Flow of magnetic shear thinning nano fluid under zero mass flux and hall current. *J. Mol. Liq.* **2022**, *352*, 118732. [[CrossRef](#)]
10. Balaji, T.; Rajendiran, S.; Selvam, C.; Lal, D.M. Enhanced heat transfer characteristics of water based hybrid nanofluids with graphene nanoplatelets and multi walled carbon nanotubes. *Powder Technol.* **2021**, *394*, 1141–1157. [[CrossRef](#)]
11. Manohar, G.R.; Venkatesh, P.; Gireesha, B.J.; Madhukesh, J.K.; Ramesh, G.K. Dynamics of hybrid nanofluid through a semi spherical porous fin with internal heat generation. *Partial. Differ. Equ. Appl. Math.* **2021**, *4*, 100150. [[CrossRef](#)]
12. Chen, Y.; Luo, P.; Tao, Q.; Liu, X.; He, D. Natural convective heat transfer investigation of nanofluids affected by electrical field with periodically changed direction. *Int. Commun. Heat Mass Transf.* **2021**, *128*, 105613. [[CrossRef](#)]
13. Jaafar, A.; Jamaludin, A.; Nasir, N.A.A.M.; Nazar, R.; Pop, I. MHD opposing flow of Cu–TiO₂ hybrid nanofluid under an exponentially stretching/shrinking surface embedded in porous media with heat source and slip impacts. *Results Eng.* **2023**, *17*, 101005. [[CrossRef](#)]
14. Mustafa, J.; Abdullah, M.M.; Ahmad, M.Z.; Husain, S.; Sharifpur, M. Numerical study of two-phase turbulence nanofluid flow in a circular heatsink for cooling LEDs by changing their location and dimensions. *Eng. Anal. Bound. Elem.* **2023**, *149*, 248–260. [[CrossRef](#)]
15. Zainal, N.A.; Waini, I.; Khashi'ie, N.S.; Kasim, A.R.M.; Naganthran, K.; Nazar, R.; Pop, I. Stagnation point hybrid nanofluid flow past a stretching/shrinking sheet driven by Arrhenius kinetics and radiation effect. *Alex. Eng. J.* **2023**, *68*, 29–38. [[CrossRef](#)]
16. Abdollahi, S.A.; Alizadeh, A.A.; Esfahani, i.C.; Zarinfar, M.; Pasha, P. Investigating heat transfer and fluid flow betwixt parallel surfaces under the influence of hybrid nanofluid suction and injection with numerical analytical technique. *Alex. Eng. J.* **2023**, *70*, 423–439. [[CrossRef](#)]
17. Shahzad, A.; Imran, M.; Tahir, M.; Khan, S.A.; Akgül, A.; Abdullaev, S.; Park, C.; Zahran, H.Y.; Yahia, I.S. Brownian motion and thermophoretic diffusion impact on Darcy-Forchheimer flow of bioconvective micropolar nanofluid between double disks with Cattaneo-Christov heat flux. *Alex. Eng. J.* **2023**, *62*, 1–15. [[CrossRef](#)]
18. Kairi, R.R.; Roy, S.; Raut, S. Stratified thermosolutal Marangoni bioconvective flow of gyrotactic microorganisms in Williamson nanofluid. *Eur. J. Mech. B/Fluids* **2023**, *97*, 40–52. [[CrossRef](#)]
19. Hussain, S.; Aly, A.M.; Alsedias, N. Bioconvection of oxytactic microorganisms with nano-encapsulated phase change materials in an omega-shaped porous enclosure. *J. Energy Storage* **2022**, *56*, 105872. [[CrossRef](#)]
20. Din, I.S.U.; Siddique, I.; Ali, R.; Jarad, F.; Abdal, S.; Hussain, S. On heat and flow characteristics of Carreau nanofluid and tangent hyperbolic nanofluid across a wedge with slip effects and bioconvection. *Case Stud. Therm. Eng.* **2022**, *39*, 102390. [[CrossRef](#)]
21. Mariam, A.; Siddique, I.; Abdal, S.; Jarad, F.; Ali, R.; Salamat, N.; Hussain, S. Bioconvection attribution for effective thermal transportation of upper convected Maxwell nanofluid flow due to an extending cylindrical surface. *Case Stud. Therm. Eng.* **2022**, *34*, 102062. [[CrossRef](#)]
22. Cui, J.; Munir, S.; Raies, S.F.; Farooq, U.; Razzaq, R. Non-similar aspects of heat generation in bioconvection from flat surface subjected to chemically reactive stagnation point flow of Oldroyd-B fluid. *Alex. Eng. J.* **2022**, *61*, 5397–5411. [[CrossRef](#)]
23. Habib, D.; Abdal, S.; Ali, R.; Baleanu, D.; Siddique, I. On bioconvection and mass transpiration of micropolar nanofluid dynamics due to an extending surface in existence of thermal radiations. *Case Stud. Therm. Eng.* **2021**, *27*, 101239. [[CrossRef](#)]
24. Waqas, H.; Naseem, R.; Muhammad, T.; Farooq, U. Bioconvection flow of Casson nanofluid by rotating disk with motile microorganisms. *J. Mater. Res. Technol.* **2021**, *13*, 2392–2407. [[CrossRef](#)]
25. Baranovskii, E.S. Flows of a polymer fluid in domain with impermeable boundaries. *Comput. Math. Math. Phys.* **2014**, *54*, 1589–1596. [[CrossRef](#)]
26. Muzara, H.; Shateyi, S. MHD Laminar Boundary Layer Flow of a Jeffrey Fluid Past a Vertical Plate Influenced by Viscous Dissipation and a Heat Source/Sink. *Mathematics* **2021**, *9*, 1896. [[CrossRef](#)]
27. Raje, A.; Bhise, A.A.; Kulkarni, A. Entropy analysis of the MHD Jeffrey fluid flow in an inclined porous pipe with convective boundaries. *Int. J. Therm.* **2023**, *17*, 100275. [[CrossRef](#)]
28. Khan, Z.A.; Shah, N.A.; Haider, N.; El-Zahar, E.R.; Yook, S.J. Analysis of natural convection flows of Jeffrey fluid with Prabhakar-like thermal transport. *Case Stud. Therm. Eng.* **2022**, *35*, 102079. [[CrossRef](#)]
29. Nabwey, H.A.; Mushtaq, M.; Nadeem, M.; Ashraf, M.; Rashad, A.M.; Alshber, S.I.; Hawsah, M.A. Note on the Numerical Solutions of Unsteady Flow and Heat Transfer of Jeffrey Fluid Past Stretching Sheet with Soret and Dufour Effects. *Mathematics* **2022**, *10*, 4634. [[CrossRef](#)]
30. Ahmad, I.; Aziz, S.; Ali, N.; Khan, S.U. Radiative unsteady hydromagnetic 3D flow model for Jeffrey nanofluid configured by an accelerated surface with chemical reaction. *Heat Transf. Asian Res.* **2021**, *50*, 942–966. [[CrossRef](#)]
31. Liao, S.J. On the Analytic Solution of Magnetohydrodynamic Flows of non-Newtonian Fluids over a stretching sheet. *J. Fluid Mech.* **2003**, *488*, 189–212. [[CrossRef](#)]
32. Turkyilmazoglu, M. Numerical and Analytical solutions for the Flow and Heat Transfer near the Equator of an MHD Boundary layer over a Porous Rotating sphere. *Int. J. Therm. Sci.* **2011**, *50*, 831–842. [[CrossRef](#)]
33. Abbasbandy, S.; Shirzadi, A. Homotopy Analysis Method for a Nonlinear Chemistry Problem. *Stud. Nonlinear Sci.* **2010**, *1*, 127–132.

34. Dinarvand, S.; Abbassi, A.; Hosseini, R.; Pop, I. Homotopy analysis method for mixed convective boundary layer flow of a nanofluid over a vertical circular cylinder. *Therm. Sci.* **2015**, *19*, 549–561. [[CrossRef](#)]
35. Ariel, P.D. The three-dimensional flow past a stretching sheet and the homotopy perturbation method. *Comput. Math. Appl.* **2007**, *54*, 920–925. [[CrossRef](#)]

Disclaimer/Publisher’s Note: The statements, opinions and data contained in all publications are solely those of the individual author(s) and contributor(s) and not of MDPI and/or the editor(s). MDPI and/or the editor(s) disclaim responsibility for any injury to people or property resulting from any ideas, methods, instructions or products referred to in the content.